NUCL SCI TECH (2016) 27:67
DOI 10.1007/s41365-016-0063-0

Ballistic deficit compensation method for a large-volume HPGe detector at high count rates

Chuan-Yun Xiong[1,2] · Ming-Zhe Liu[1,2] · Zhuo Zuo[1,2] · Xian-Guo Tuo[1]

Received: 17 August 2015 / Revised: 28 September 2015 / Accepted: 6 October 2015 / Published online: 12 May 2016

Abstract A large-volume HPGe detector normally has a severe ballistic deficit due to its long rise time of the output signals. Despite the trapezoidal shaping algorithm adopted as a remedy to deal with the signals, the algorithm cannot fully eliminate the ballistic deficit in the case of a high counting rate. To resolve the problem, we propose a ballistic deficit compensation method that is based on the measurement of rise time of the signals before shaping. We find that the ballistic deficit after trapezoidal shaping has little relation to the time constant, but shows a quadratic relationship with the rise time and has a negative correlation with the shaping time. In the case of high count rates, the high resolution is handled by fitting the curve to the rise time and the amplitude deficit of the signal after shaping and by compensating for the signal amplitude after trapezoidal shaping. Tests indicate that when the count rate is about 100 kcps, the resolution of Co-60 improves from traditional 2.32 up to 1.91 keV, thus reaching a higher level.

This work was supported by Natural Science Foundation of China (No. 41274109) and Youth Innovation Team of Sichuan Province (2015TD0020).

✉ Ming-Zhe Liu
liumz@cdut.edu.cn

Chuan-Yun Xiong
854314483@qq.com

[1] State Key Laboratory of Geohazard Prevention and Geoenvironment Protection, Chengdu University of Technology, Chengdu 610059, China

[2] College of Nuclear Technology and Automation Engineering, Chengdu University of Technology, Chengdu 610059, China

Keywords HPGe detector · Ballistic deficit · Trapezoidal shaping algorithm · Rise time measurement · Amplitude compensation

1 Introduction

The high-purity germanium (HPGe) detector has served as an indispensable part of some gamma rays and X-ray spectroscopic technology and products. Gamma rays and X-rays are important tools for studying nuclear physics and nuclear reactions, such as nuclear structure, molecular physics, and atomic collision. This detector has been widely applied across multiple disciplines including nuclear power, environment, inspection and quarantine, biological medicine, celestial physics and chemistry, geology, law, archeology, and metallurgy and materials science [1–3].

Because an HPGe detector has a long charge collection time and a broad width for the signal rise time, a long shaping time is needed to deal with the signal [4, 5] so that ballistic deficit can be mitigated. If the shaping time is long, it will curb the counting rate of the detector and thereafter confine its applications [6, 7].

Although numerous methods have been used to reduce the ballistic deficit and improve energy resolution, the compensation method for the ballistic deficit in the case of high counting rates is rarely studied. Based on the hardware circuit, a simulated correction circuit was designed to correct the obtained signal amplitude [8]. This method performed well, but was inconvenient [8, 9], because its hardware structure was extremely complex and the method had to adjust the parameters of the hardware for detectors of different sizes. Tennelec and Ortec produced a multi-

channeled detecting system to obtain diverse energy resolutions in the case of different counting rates without using a specific method to improve energy resolution [4]. A double-class shaping method was introduced for large-volume HPGe, where the bottom of the shaping signal used pinnacle shaping and the top of the shaping signal used parabola shaping. This is a good method to curb the signal noise and compensate to some extent for the ballistic deficit. Compared with standard Gaussian shaping, this method pushed the noise factor up by 10 %–12 %. However, it works only in the case of low count rates and cannot fully eliminate the ballistic deficit [10].

To resolve this problem, we propose a compensation method for ballistic deficit when the shaping time is short, so that the large-volume HPGe detector can achieve good energy resolution when the counting rate is high.

2 Operating principle of the large-volume HPGe detector

Because the large-volume HPGe detector has an overly large and sensitive volume and the hole–electron pairs that are produced after the gamma ray enters the detector require a long time to be collected by the electrode, the output pulse of the detector has a broad range in rise time fluctuation (as shown in Fig. 1). Figure 1a is the cross-sectional drawing of the P-type coaxial single open-ended HPGe detector with a diameter of 70 mm and a height of 82.6 mm; Fig. 1b is a schematic of the charge that is formed by the gamma ray at different locations; Fig. 1c is the schematic of the voltage [11] which is formed by the charge after going through the charge-sensitive amplifier and the CR (capacitor and resistor) differentiating circuit as shown in Fig. 2.

In Fig. 1, point A stands for the time shared by the two motions: that from the hole to cathode and that from electron to anode. This signal has the shortest rise time. Because point B is closer to the anode, the electron is collected by the anode immediately after it is produced, while the hole cannot be collected by the cathode until it has traveled a long distance (the radius, about 35 mm). The signal thus has the longest rise time. Point C is in between A and B. It can be seen from the figure that the rise time of the input signal of the large-volume HPGe detector is long and changes widely (T_{min}–T_{max}), causing the signal to leave a more serious ballistic deficit after going through the CR differentiating circuit shown in Fig. 2.

The charge at point A, point B, or point C is formed by single hole–electron pairs. Actually when gamma rays enter the detector producing large amounts of hole–electron pairs, the curve D in Fig. 1b presents the result of the accumulative effects of all the hole–electron pairs [11].

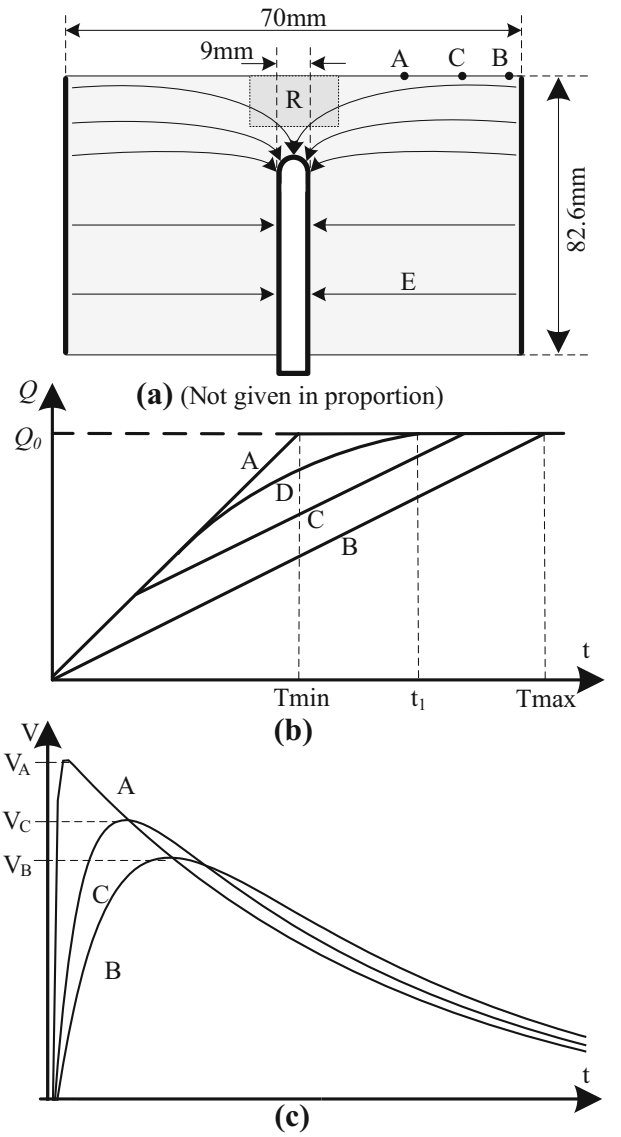

Fig. 1 Operating principle schematic

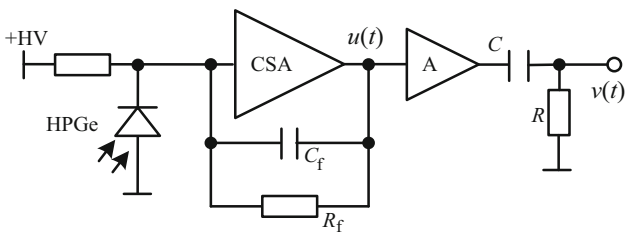

Fig. 2 Signal conditioning circuit of the HPGe detector

3 Ballistic deficit of the large-volume HPGe detector

The relationship between the ballistic deficit in the CR differentiating circuit (in Fig. 2) and signal rise time is derived as follows. The output charge of the detector is given by Wang et al. [12] as Eq. (1):

$$Q(t) = Q_0(1 - e^{-t/\tau_0}) \tag{1}$$

where Q_0 stands for the maximum output charge produced by the gamma ray entering the detector and τ_0 is the duration of the time constant of the signal before shaping (the time constant) of the output charge. The output current $i(t)$ of the detector is given by Eq. (2):

$$i(t) = \frac{Q_0}{\tau_0} e^{-t/\tau_0} \tag{2}$$

By integrating the feedback capacitance C_f of the charge-sensitive amplifier shown in Fig. 2, we obtain the output voltage signal $u(t)$ from the output current $i(t)$ of the detector. This also releases a part of the charge through the feedback resistance R_f. The differential Eq. (3) is as follows:

$$C_f u(t) = \int_0^t I(t)dt - \int_0^t \frac{u(t)}{R_f} dt \quad (0 \le t \le t_1) \tag{3}$$

In the case of the initial condition where $t = 0$, $u(t) = 0$, $u(t)$ is given by Eq. (4):

$$u(t) = \frac{Q_0}{C_f \tau_0} \times \frac{1}{\frac{1}{R_f C_f} - \frac{1}{\tau_0}} \times \left(e^{\frac{-t}{\tau_0}} - e^{\frac{-t}{R_f C_f}}\right) \tag{4}$$

The relationship between the voltage signal $v(t)$ following the CR differential circuit and $u(t)$ is given by Eq. (5):

$$v(t) = u(t) - \int_0^t \frac{v(t)}{CR} dt \quad (0 \le t \le t_1) \tag{5}$$

In the case of the initial condition where $t = 0$, $v(t) = 0$, $v(t)$ is given by Eq. (6):

$$v(t) = \frac{Q_0}{C_f \tau_0} \times \frac{1}{\frac{1}{R_f C_f} - \frac{1}{\tau_0}} \times \left(\frac{1}{R_f C_f} \times \frac{1}{\frac{1}{RC} - \frac{1}{R_f C_f}} \times \left(e^{-t/R_f C_f} - e^{-t/RC}\right) + \frac{1}{\tau_0} \times \frac{1}{\frac{1}{RC} - \frac{1}{\tau_0}} \times \left(e^{-t/RC} - e^{-t/\tau_0}\right) \right) \tag{6}$$

After determining the derivative of Eq. (6), t_r (the rise time of $v(t)$) is the maximum of $v(t)$ when $v'(t) = 0$, and then, t_r is put into Eq. (6) to get $v_{max}(t)$ which is the maximum of $v(t)$. Due to the ballistic deficit, $v_{max}(t)$ is less than Q_0/C_f. The signal amplitude deficit η is given by Eq. (7):

$$\eta(tr) = 1 - \frac{v_{max}(t)}{Q_0/C_f} = 1 - \frac{1}{\tau_0} \times \frac{1}{\frac{1}{R_f C_f} - \frac{1}{\tau_0}} \times \left(\frac{1}{R_f C_f} \times \frac{1}{\frac{1}{RC} - \frac{1}{R_f C_f}} \times \left(e^{-t_r/R_f C_f} - e^{-t_r/RC}\right) + \frac{1}{\tau_0} \times \frac{1}{\frac{1}{RC} - \frac{1}{\tau_0}} \times \left(e^{-t_r/RC} - e^{-t_r/\tau_0}\right) \right) \tag{7}$$

Suppose that $R_f C_f = 100$ μs, then Fig. 3 shows the relationship between the amplitude deficit η of the circuit and the signal rise time when the differentiating time constant τ varies. Figure 3 indicates that the higher the signal rise time, the more serious the ballistic deficit, while the lower the CR time constant τ, the larger the ballistic deficit. When the CR time constant τ is 1.02 μs, the ballistic deficit ranges from 11 % to 39 % if the rise time of the signal output of the HPGe detector fluctuates from 120 to 500 ns. It can be seen that the ballistic deficit increases with the increase in rise time, so that the energy resolution of the system becomes worse.

4 The inhibition ability of the ballistic deficit of the trapezoidal shaping algorithm

To curb the influence of the circuit ballistic deficit on the energy resolution of the system, the output signal of the detector is processed with a trapezoidal shaping algorithm which has a low-pass filter that performs increasingly better as the rising edge of the trapezoidal gets broader.

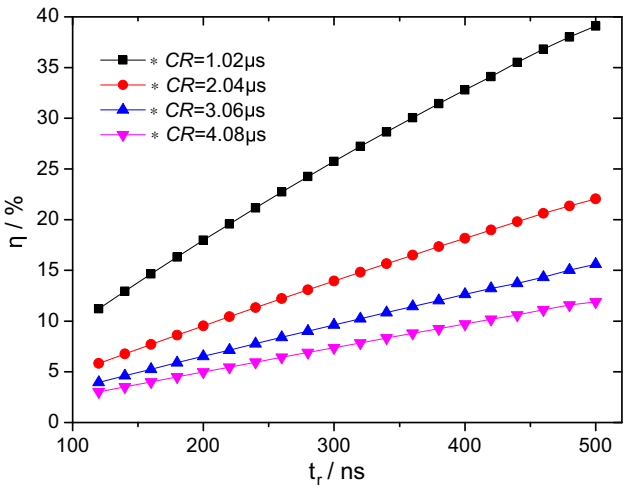

Fig. 3 Amplitude deficit η of the signal when time constant τ in the circuit

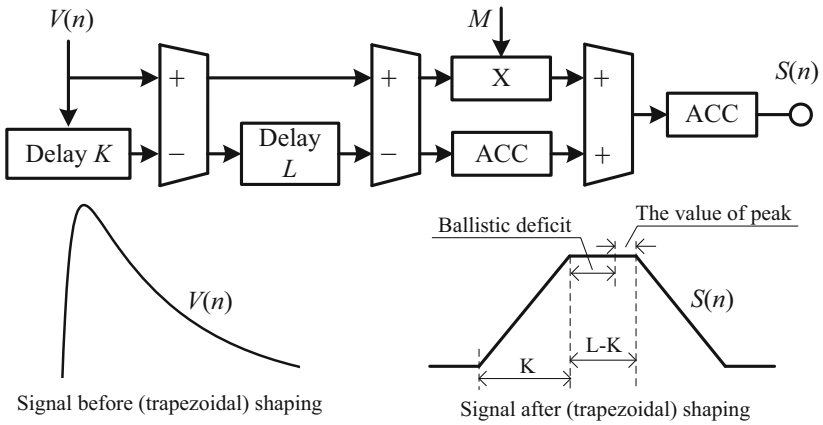

Fig. 4 Block diagram of the trapezoidal shaping algorithm

When the width of the trapezoidal flat top surpasses the maximum charge collection time of the detector, the algorithm has improved immunity to the ballistic deficit [13–16]. The block diagram of the trapezoidal shaping algorithm is shown in Fig. 4 where $V(n)$ stands for the pulse signal before trapezoidal shaping that is discretized by a high-speed ADC, and $S(n)$ symbolizes the signal after trapezoidal shaping. The parameter M depends on the time constant τ of the input signal $V(n)$ as defined by Eq. (8), and M determines the trapezoidal shape.

$$M = \frac{1}{e^{T_{clk}/\tau - 1}} \tag{8}$$

T_{clk} stands for the sampling period of the ADC.

Parameter K decides the trapezoidal rise time (that is the signal shaping time T_s), and parameter L determines the trapezoidal rise time plus flat top time. The longer T_s is, the larger the signal amplitude after shaping is and the stronger the inhibiting ability on the noise is. Because an extremely long shaping time reduces the counting rate of the system, it is necessary to identify a suitable value. If the input signal ($V(n)$) has a long rise time, such as 500 ns, the signal after shaping is not a standard trapezoid. The first part of the trapezoidal flat top cannot represent the real signal amplitude as it presents a downward trend due to the ballistic deficit, and the latter part of the flat part approximates the real signal amplitude. Therefore, in the real-world applications when the flat top time is greater than the maximum rise time of pulse signal, the ballistic deficit can be inhibited.

Actually, the trapezoidal shaping algorithm is unable to fully eliminate the ballistic deficit. As for the inhibiting ability of the trapezoidal shaping algorithm on the ballistic deficit, we have reached two conclusions: First, when T_s remains at the same value, the signal before shaping at different time constants τ has the same ballistic deficit after trapezoidal shaping. In other words, the ballistic deficit of the signal after trapezoidal shaping is completely independent of τ (refer to Table 1 for details). However, in the circuit shown in Fig. 2, the ballistic deficit before shaping

Table 1 Ballistic deficits η of the signals after shaping of different time constants at diverse shaping times

Rise time/t_r (ns)	Deficit of the shaping time of 1.02 μs/η (%)		Deficit of the shaping time of 2.04 μs/η (%)		Deficit of the shaping time of 3.06 μs/η (%)		Deficit of the shaping time of 4.08 μs/η (%)	
	τ = 1.02 μs	τ = 4.08 μs	τ = 1.02 μs	τ = 4.08 μs	τ = 1.02 μs	τ = 4.08 μs	τ = 1.02 μs	τ = 4.08 μs
100	0.081286	0.078762	0.089234	0.086687	0.064826	0.059274	0.060011	0.061091
140	0.164697	0.159818	0.127325	0.119420	0.081537	0.079625	0.079201	0.080642
180	0.380391	0.376548	0.233565	0.228709	0.151639	0.149751	0.132671	0.133087
220	0.753885	0.748347	0.421365	0.415785	0.277074	0.276474	0.227185	0.228313
260	1.287326	1.282699	0.694625	0.689947	0.460325	0.460614	0.364771	0.365008
300	1.967420	1.963467	1.057278	1.053202	0.699834	0.700773	0.544352	0.543938
340	2.773437	2.770003	1.483866	1.480364	0.991930	0.993361	0.763250	0.762340
380	3.682695	3.679674	1.980029	1.976931	1.327846	1.329663	1.015006	1.013708
420	4.670482	4.667796	2.537430	2.534662	1.707455	1.709580	1.299673	1.298062
460	5.722376	5.719968	3.148300	3.145805	2.126360	2.128735	1.614168	1.612302
500	6.823959	6.821786	3.805044	3.802780	2.580363	2.582943	1.955615	1.953538
540	7.994782	7.993659	4.503627	4.500629	3.086802	3.083745	2.314590	2.321382

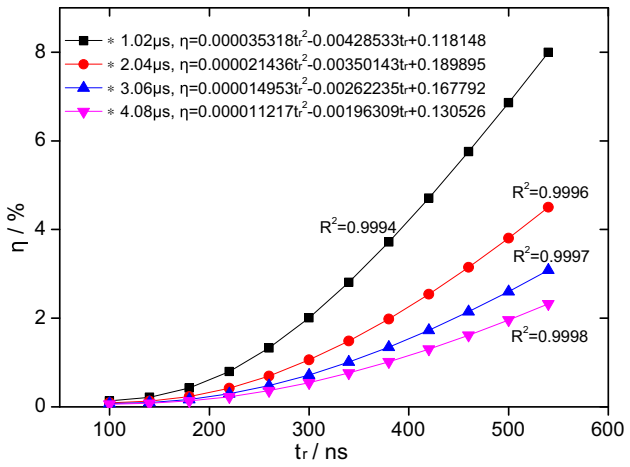

Fig. 5 Amplitude deficit η of signal after shaping at different shaping times

is inversely related to the time constant τ (see Fig. 3 for details). It follows that the trapezoidal shaping algorithm is immune to the changes of the time constant τ. Secondly, the ballistic deficit decreases along with the increasing shaping time (more details are explained in Table 1 and Fig. 5).

In the case when the sampling rate of the ADC is 40 MHz and the flat top time is 1.05 μs, the ballistic deficits of the signals of different time constants τ (1.02, 2.04, 3.06, and 4.08 μs) are, respectively, studied over diverse shaping times T_s (1.02, 2.04, 3.06, 4.08 μs). To keep the explanations concise and simple, Table 1 just lists the data for $\tau = 1.02$ μs and 4.08 μs. It can be seen that the ballistic deficit of the signal after shaping has little bearing on the time constants τ of the signal before shaping, but has a tighter relationship with shaping times T_s.

Figure 5 illustrates the amplitude deficit η of the signal after shaping at different shaping time T_s. It can be seen from Fig. 5 that if the shaping time is relatively long, such as 4.08 μs, the signal amplitude deficit is less than 2 % when the rise time of the signal before shaping (the rise time) is 500 ns. The experiment proves that if the shaping time is over 8 μs, the signal amplitude deficit is less than 1 % when the rise time is 500 ns. On the other hand, if the shaping time is relatively short, such as 1.02 μs, the signal amplitude deficit reaches up to 6.86 % when the rise time is 500 ns. If the rise time of the signal output of the HPGe detector ranges from 150 ns to 500 ns, the amplitude deficits η are confined to the range from 0.21 % to 6.86 %. Because the energy resolution of HPGe detector is intrinsically high, it will be negatively affected to a large extent by the changes of the ballistic deficit mentioned above.

Coupled with the longer shaping time, the inhibiting ability of trapezoidal shaping has a stronger effect on the ballistic deficit, while the counting rate is reducing. Applications with a high count rate require less shaping time, and when the inhibiting ability of the trapezoidal shaping on ballistic deficit is receding, the effect of the ballistic deficit on the system energy resolution is more obvious. To adjust for applications with high counting rates, a new compensation method is put forward based on the trapezoidal shaping algorithm. The shaped signal amplitude deficit is compensated by measuring the rise time of the signal before shaping and adopting the fit shown in Fig. 5 to allow the system to obtain a higher energy resolution even when the counting rate is high.

The curves at different shaping times show that the ballistic deficit η after shaping has a quadratic relationship with the rise time and that the fit is good. Thus, this polynomial fit facilitates the compensation for ballistic deficit, so that the system has a good energy resolution in the case of high counting rates. The curve fit improves with the rise of the shaping time T_s, because the longer the shaping time is, the better the filtering effect is because it is less affected by the signal noise. Therefore, the fit improves.

In addition, according to the data in Table 1, when the rise time stays relatively short, such as 100 ns or 140 ns, the ballistic deficits of the signals after shaping on different time constants τ have small differences from each other. But this does not affect the accuracy of our compensation method. On the one hand, the rise time of the minimum output signal of the large-volume HPGe detector is about 180 ns (see detail in Fig. 9). Under this circumstance, the signal amplitude deficit values of different time constants τ are basically the same after shaping without great changes. On the other hand, when the rise time is short, the ballistic deficit after shaping is intrinsically low in value (<0.5 %); thus, the error here has little influence on the overall amplitude compensation.

Besides, because the ballistic deficit after shaping has nothing to do with the time constant τ (CR differentiating time constant in the hardware circuit) of the signal before shaping, this compensation method can be unfettered to a large extent from the circuit. This method requires adjusting the rise time T_s in accordance with the count rate rather than considering the adjustment of the parameters of the hardware circuit. Therefore, this is a convenient method without complicated debugging of the hardware circuit. And the appropriate adjustment of the CR time constant τ in the hardware circuit can equip the signal with narrower pulse width and improve the counting pass rate of the circuit. The selected CR time constant τ is 3.2 μs in this paper.

5 Ballistic deficit compensation method based on rise time measurement

To handle applications with high counting rates in this article, we present a ballistic deficit compensation method based on rise time measurement. The basic idea of this

method is as follows: First, the rise time of the signal before shaping is measured with a double-channel trapezoidal shaping module. Second, the amplitude deficit of the signal after shaping is obtained at a specified shaping time in accordance with the rise time through the relationship shown in Fig. 5. Finally, to generate an amplitude spectrum, a channel conversion is performed after compensating for the amplitude of the sampling signal. The key point of this method is the rise time measurement. The measurement accuracy of the signal rise time directly affects the compensation precision. Let us start with the implementations of the rise time measurement in this method.

5.1 Rise time measuring module

The rise time measuring module is shown in Fig. 6. The core of this module is a double-channel digital trapezoidal shaper where one of the channels is a fast shaping path with the fixed shaping time T_s of 150 ns and the flat top time of 200 ns, and the other channel is an adjustable slow shaping channel with the shaping time adjustable from 1 μs to 12 μs. When the optimal shaping time of the slow channel is determined, if the rise time of the signal before shaping is the same, then the amplitude ratio between the slow channel and the fast channel (*RATIO*) is constant. The shorter the rise time of the signal before shaping, the lower the *RATIO*, while the longer the former is, the higher the latter turns out to be. What leads to this situation is that the shaping time of the fast channel can be as short as 150 ns, so when the slowly rising signal goes through the fast channel, the rising edge of the signal before shaping is not fully integrated and the amplitude of the signal after shaping is smaller; however, the signal through the slow channel can be fully integrated and its value basically remains unchanged, and thus, the *RATIO* increases. Therefore, this system can be employed as long as the relationship linking the rise time of the signal before shaping with the *RATIO* is in accordance with the different shaping times of the slow channel.

The curve that fits the *RATIO* and rise time is greatly affected by the shaping time T_s and flat top time of the fast channel. When the shaping time T_s and flat top time vary, the fitting curve may be cubic, quadratic, or linear. It is essential to select the appropriate shaping time T_s and flat top time in the fast channel. If the shaping time of the fast channel is too short, the filter performance is injured and the noise has a greater influence on the amplitude of the fast channel, while if the shaping time is extremely long, the *RATIO* will shrink and show little change when the signal rise time varies. As a result, when fitting the signal rise time and the *RATIO*, the coefficients of the fitting polynomial must retain more valid data; this may be detrimental to arithmetical operation. The meticulously selected shaping time and flat top time are 150 and 200 ns, respectively, to ensure that the fast channel is not affected by noise on the one hand, and allow the *RATIO* to change in a more obvious way along with the change of rise time on the other hand. This makes the arithmetic operation more convenient and improves the accuracy of the computation results.

The trapezoidal shaping time of the fast channel is 150 ns, and the flat top time is 200 ns. The flat top time of the trapezoidal shaping of the slow channel is 1.05 μs, with the constantly changing rise time (100–660 ns) of the input signal. The relationship between the signal rise time and the *RATIO* can be measured at different shaping times of the slow channel. When the *RATIO* is as low as a single double digit and the rise time is as high as a three digit in ns, it is necessary to multiply the *RATIO* by 1000 before fitting for the sake of convenient computation and accurate fitting functions. The result is shown in Fig. 7. The curve approximates linearity, but the system introduces a quadratic curve to improve fitting performance and the precision of the rise time computation.

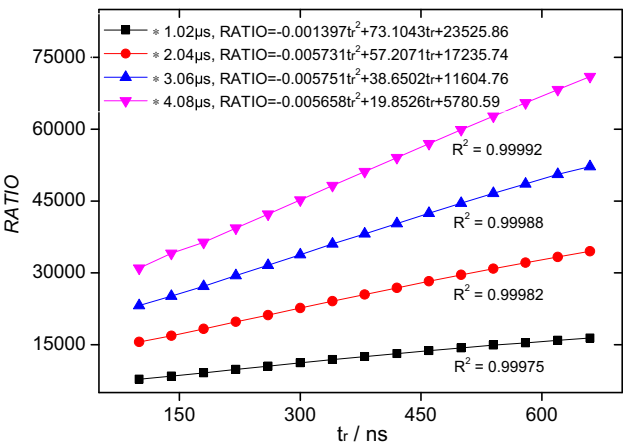

Fig. 7 Relationship between the RATIO and rise time of signal before shaping

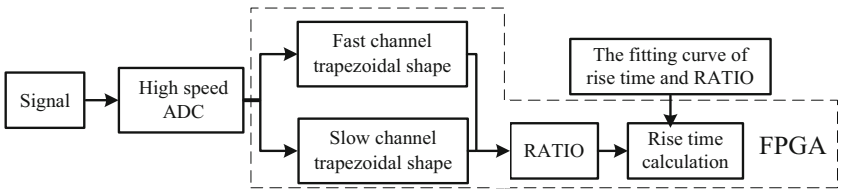

Fig. 6 Schematic diagram of rise time measuring module

In addition, Fig. 7 indicates that the fit between the signal rise time and the *RATIO* improves along with longer shaping time in the slow shaping channel. Therefore, in the real-world application, if the counting rate is not high, it is suggested that the shaping time of the slow channel be extended in the rise time measuring module to improve the measuring accuracy of the rise time.

5.2 Amplitude compensation method

Figure 8 shows the operational schematic diagram of the amplitude compensation method. This method adds an extra amplitude compensation module, which further decreases the ballistic deficit of the signal and improves the energy resolution of the system. The following is the working principle: After determining the signal shaping time of the slow channel, the rise time is measured through the rise time measurement module, and the ballistic deficit is obtained under the rise time of the signal according to the relationship shown in Fig. 5. To decrease the signal's ballistic deficit and improve the system's energy resolution, the amplitude is extracted from the slow channel and compensated based on the ballistic deficit value calculated above.

6 Results and discussion

The detector used in the experiment is a P-type signal-start coaxial HPGe detector as shown in Fig. 1a. We are going to measure the rise time spectrum of the detector's output signal and the energy resolution of the signal amplitude spectrum under a relatively higher counting rate, respectively.

6.1 The rise time spectrum of the detector's output signal

To compensate for the ballistic deficit caused by the rise time change of the detector's output signal, we should first know the rise time of the output signal. At the same time, by measuring the rise time distribution of the output signal, we are able to find out the characteristics of the output signal as well as measure the performance of the rise time measurement module in the system.

Figure 9 shows the rise time spectrum of the measurement of the detector's output signal on the condition that the CR time constant τ is 3.2 μs and the slow channel shaping time is 4.08 μs in the rise time measurement module. A Co-60 source is used in the measurement, and the source and detector are 40 cm apart. The bias voltage is 2600 V; the counting rate is about 6.2 kcps, with a measuring time of 180 s and ADC sample rate of 40 MHz.

As shown in Fig. 9, the rise time of the HPGe detector's output signal is distributed between 180 and 540 ns, and the signal rise time is uniformly distributed between 210 and 400 ns. This is because the radioactive source and detector are far enough apart, so we can assume that rays enter the detector evenly. Therefore, the hole–electron pairs generated in the detector are evenly distributed, as is the signal rise time. When the rise time is between 440 and 460 ns, there is a small flat area in the spectral lines. Meanwhile, there is a long trailing section on the right side of the time spectrum when the rise time is relatively large. Due to the fact that this is a single-start detector, the electric field intensity is relatively weak near the axis of the

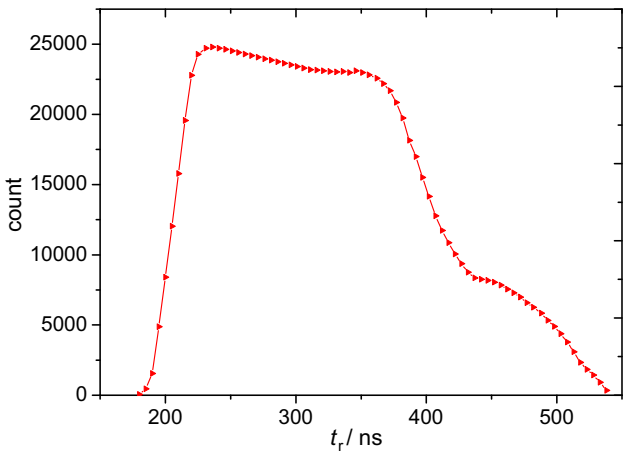

Fig. 9 Rise time spectrum of the HPGe detector output signal

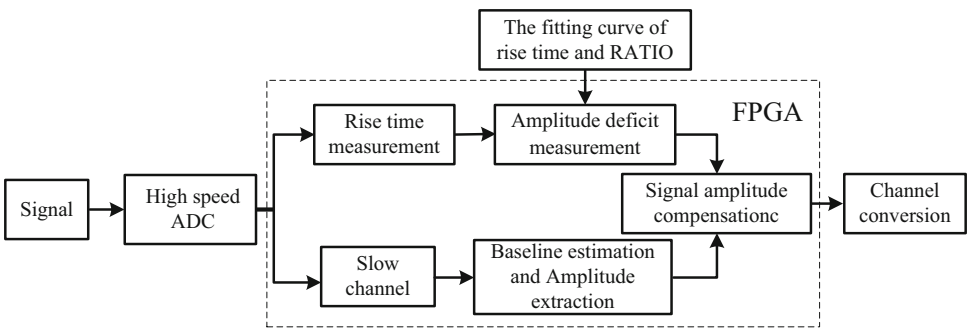

Fig. 8 Operation schematic diagram of the amplitude compensation method

side with no start. This is shown as *R* and its adjacent area in Fig. 1a, and the drift velocity of hole–electron pairs generated in this area is slow. Thus, the rise time of the signal generated in this area is longer, and there is a small step on the time spectrum.

6.2 The energy resolution of the system at high count rates

Figure 10 shows the effect of adopting this compensation method on system resolution for Co-60 source under different counting rate conditions. Under different circumstances, the counting rate used in the system is not the same. When the counting rate is lower than 3 kcps, the shaping time becomes 12 μs; when the counting rate is between 3 and 10 kcps, the shaping time becomes 8 μs; when the counting rate is between 10 and 40 kcps, the shaping time becomes 6 μs; when the counting rate is between 40 and 80 kcps, the shaping time becomes 4 μs; when the counting rate is between 80 kcps and 150 kcps, the shaping time becomes 2 μs; and when the counting rate is over 150 kcps, the shaping time becomes 1 μs. See the details in Fig. 10.

As can be seen from the figure, the system's resolution has been improved after adopting the compensation method. When the counting rate is relatively low, the system resolution for a 1.33 MeV gamma ray can reach 1.82 keV. With the increase in counting rate, the shaping time decreases in the system and ballistic deficit tends to become more and more serious. Without this compensation method, the system's resolution decreases as the counting rate increases. When the shaping time is the same, the system's resolution obviously does not change with the change in counting rate. The reason for this is that the amplitude deficit of the signal after shaping is basically the same when the shaping time is the same.

By adopting this compensation method, the amplitude deficit due to the shorter shaping time is balanced, which enables a better resolution at high count rates. However, the system's resolution still tends to worsen slightly with the increase in counting rate. This is because the higher the counting rate, the shorter the shaping time of slow channel in the rise time measurement module, the slight worsening in the accuracy of the rise time measurement is sure to result in the accuracy of the amplitude compensation declining slightly.

6.3 The relationship between system counting throughput rate and counting rate

To access the effect of pile-up pulse on the system's counting throughput rate, namely the detection efficiency of the detector under high counting rate circumstances, we plot the relationship in Fig. 11 which shows the relationship between the system's counting throughput rate and the counting rate when the flat top time of the trapezoid is 1.05 μs and the shaping time varies. As seen in the figure, the counting throughput rate of the system decreases as the counting rate increases and reduces with increasing shaping time.

In addition, although the counting rate of the system can reach 150 kcps when the shaping time is minor, the practical counting throughput rate is not that high since the signal piles up a lot when counting rate is too high. The system's counting throughput rate is only about 73 % when the shaping time is 1.02 μs and the counting rate is 150 kcps. Thus, in practical applications, we should compensate for the discarded pulse because of pulse pile-up in accordance with the curve given in Fig. 11. The compensation method is as follows: When the shaping time of the system is determined, one can obtain any spectrum by measuring, and calculate the counting rate of the spectrum,

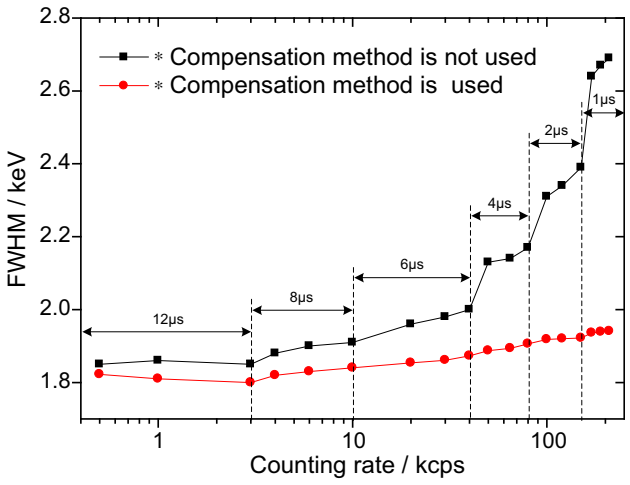

Fig. 10 Curves between the system resolution and the counting rate

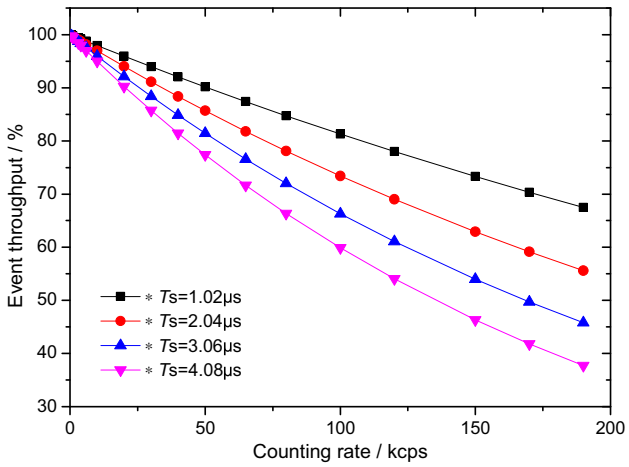

Fig. 11 Relationship between system counting throughput rate and counting rate

and obtain the counting throughput rate according to the curve shown in Fig. 11. Finally, one can compensate for the counting rate according to the probability density distribution function of the spectrum.

The premise to compensate for the counting rate according to the probability density distribution function is that the probability density function of the discarded pulse signal has the same distribution as the spectrum which is obtained by measuring. In fact during the probe of the high counting rate, when the counting of the spectrum increases to a high level in a short period of time, the influence of the statistical fluctuation of the system can be ignored, so the discard pulse signal has a random distribution; it meets the premise condition. Therefore, it can compensate for the counting rate according to the probability density distribution function of the spectrum which is obtained by measuring.

7 Conclusion

In the large-volume HPGe detector because the rise time of the output signal has a large fluctuation range (from 180 to 540 ns), the ballistic deficit of the signal moves along with it and varies when the CR time constant τ changes. Although the trapezoidal shaping algorithm is immune to the time constant of the signal before shaping, the signal after shaping has a large ballistic deficit and thus turns out to be unsuitable for use with high counting rates when the shaping time is short. This is due to the defects of the algorithm itself. Thus, a ballistic deficit compensation method is suggested based on measuring the rise time. This method extracts the signal amplitude through a trapezoidal shaping algorithm and then compensates for the value of the amplitude by measuring the rise time of the signal before shaping. This method inherits the advantages of the trapezoidal shaping algorithm which is immune to the time constant τ of the signal before shaping, and also compensates for the amplitude deficit which is caused by the trapezoidal shaping algorithm itself at the high counting rate. This helps the large-volume HPGe detector achieve good energy resolution even when the counting rate is high (the shaping time is short).

The key to this compensation method is the rise time measuring module, because the measuring accuracy of the rise time directly affects the precision of the amplitude compensation. The double-channel trapezoidal shaping method is adopted to obtain the rise time of the signal before shaping. In this module, it is necessary to select a correct shaping time for the fast channel; the shorter the shaping time is, the more the noise will affect it; the longer the shaping time is, the less the *RATIO* will change, which opposes the computation of the rise time. A specialized method for measuring rise time will be the next step to improve the measuring accuracy of the signal rise time and thereafter enhance the precision of this compensation method.

References

1. X.M. Zhou, G.M. Liu, D. Li et al., Using activation method to measure neutron spectrum in an irradiation chamber of a research reactor. Nucl. Sci. Tech. **25**, 1–5 (2014). doi:10.13538/j.1001-8042/nst.25.010603
2. Shakeel Ur Rehman, Sikander M. Mirza, Nasir M. Mirza et al., GEANT4 simulation of photo-peak efficiency of small high purity germanium detectors for nuclear power plant applications. Ann. Nucl. Energy **38**, 112–117 (2011). doi:10.1016/j.anucene.2010.08.010
3. W.X. Yu, X.L. Huang, X.J. Chen et al., Evaluation of the relative γ-ray intensities emitted from Co-56 and Ga-60. Nucl. Sci. Tech. **20**, 363–368 (2009)
4. G. Duchene, M. Moszynski, Ballistic deficit correction methods for large HPGe detectors High counting rate study. Nucl. Instr. Methods A **357**, 546–558 (1995). doi:10.1016/0168-9002(95)00028-3
5. R.J. Cooper, M. Amman, P.N. Luke, K. Vetter, A prototype High Purity Germanium detector for high resolution gamma-ray spectroscopy at high count rates. Nucl. Instr. Methods A **795**, 167–173 (2015). doi:10.1016/j.nima.2015.05.0530168-9002
6. M. Nakhostin, K. Hitomi, Digital pulse processing for planar TlBr detectors, optimized for ballistic deficit and charge-trapping effect. Nucl. Instr. Methods A **675**, 47–50 (2012). doi:10.1016/j.nima.2012.02.011
7. X.Y. Wen, Y.X. Wei, W.Y. Xiao, Optimum digital filter synthesis with arbitrary constraints and noise. J. Tsinghua Univ. (Sci & Tech) **46**, 1597–1600 (2006). **(in Chinese)**
8. F.S. Goulding, D.A. Landis, Ballistic deficit correction in semiconductor spectrometers. IEEE Trans. Nucl. Sci. **35**, 119–124 (1987)
9. J. Gila, G. Hegyesi, G. Kalinka et al., Optimization of the particle discriminator based on the ballistic deficit method using delay-switched gated integrator. Nucl. Instr. Methods A **399**, 407–413 (1997). doi:10.1016/S0168-9002(97)00953-4
10. A.I. Kalinin, V.A. Bednyakov, Pulse shaping for Ge-spectrometers optimized for ballistic deficit and electronic noise. Nucl. Instr. Methods A **538**, 718–722 (2005). doi:10.1016/j.nima.2004.08.126
11. M.G. Strauss, R.N. Larsen, L. Sifter, Pulse shape distributions from gamma-rays in lithium drifted germanium detectors. IEEE Trans. Nucl. Sci. **6**, 265–273 (1996). doi:10.1016/0029-554X(67)90390-4
12. J. Wang, T.M. Fan, Y.G. Qian. *Nuclear Electronics* (Atomic Energy Press, Beijing, 1983), pp. 158–170 **(in Chinese)**
13. W.Y. Xiao, Y. Wei, X.Y. Ai, Trapezoidal shaping algorithm for digital multi-channel pulse height analysis. J. Tsing Univ. (Sci & Tech) **45**, 810–812 (2005). **(in Chinese)**
14. Cosimo Imperiale, Alessio Imperiale, On nuclear spectrometry pulses digital shaping and processing. Measurement **30**, 49–73 (2011). doi:10.1016/S0263-2241(00)00057-9
15. V.T. Jordanov, G.F. Knoll, Digital synthesis of pulse shapes in real time for high resolution radiation spectroscopy. Nucl. Instr. Methods A **345**, 337–345 (1994). doi:10.1016/0168-9002(94)91011-1
16. V.T. Jordanov, G.F. Knoll et al., Digital techniques for real-time pulse shaping in radiation measurements. Nucl Instr. Methods A **353**, 261–264 (1994). doi:10.1016/0168-9002(94)91652-7